Research Article | Vol. 26, No. 17 | 20 Aug 2018 | OPTICS EXPRESS 22378
Optics EXPRESS

20 W splice-free erbium-doped all-fiber laser operating at 1610 nm

LOUIS-PHILIPPE PLEAU,* PASCAL PARADIS, JEAN-SIMON FRENIÉRE, MATHIEU HUNEAULT, SAMUEL GOUIN, SALAH MOHAMMED ALJAMIMI, YIGIT OZAN AYDIN, SIMON DUVAL, JEAN-CHRISTOPHE GAUTHIER, JOÉ HABEL, FRÉDÉRIC JOBIN, FRÉDÉRIC MAES, LOUIS-RAFAËL ROBICHAUD, NICOLAS GRÉGOIRE, STEEVE MORENCY, AND MARTIN BERNIER

Centre d'Optique, Photonique et Lasers (COPL), Université Laval, Québec, G1V 0A6, Canada
**louis-philippe.pleau.1@ulaval.ca*

Abstract: We report on a splice-free erbium-doped all-fiber laser emitting over 20 W at a wavelength of 1610 nm, with a slope efficiency of 19.6 % and an overall efficiency of 18.3% with respect to the launched pump power at 976 nm. The simple cavity design takes advantage of fiber Bragg gratings written directly in the gain fiber through the polymer coating and clad-pumping from a single commercial pump diode to largely simplify the assembling process, making this cavity ideal for large-scale commercial deployment. Two single-mode and singly erbium-doped silica fibers were fabricated in-house: the first to assess the effects of a high erbium concentration (0.36 mol.% Er_2O_3), yielding a low efficiency of 2.5 % with respect to launched pump power, and the second to achieve the improved result mentioned above (0.03 mol.% Er_2O_3). Numerical simulations show the link between the performance of each cavity and ion pair-induced quenching.

OCIS codes: (140.3500) Lasers, erbium; (140.3510) Lasers, fiber; (230.1480) Bragg reflectors.

References and links

1. R. Frehlich, S. M. Hannon, and S. W. Henderson, "Coherent Doppler lidar measurements of winds in the weak signal regime," Appl. Opt. **36**(15), 3491–3499 (1997).
2. H. Elgala, R. Mesleh, and H. Haas, "Indoor optical wireless communication: potential and state-of-the-art," IEEE Commun. Mag. **49**(9), 56–62 (2011).
3. International Commission on Non-Ionizing Radiation Protection, "ICNIRP guidelines on limits of exposure to laser radiation of wavelengths between 180 nm and 1,000 µm," Health Phys. **105**, 271–295 (2013).
4. H. Lin, Y. Feng, Y. Feng, P. Barua, J. Sahu, and J. Nilsson, "656 W Er-doped Yb-free large-core fiber laser," Opt. Lett. **43**(13), 3080–3083 (2018).
5. Y. Jeong, S. Yoo, C. A. Codemard, J. Nilsson, J. K. Sahu, D. N. Payne, R. Horley, P. W. Turner, L. Hickey, A. Harker, and M. Lovelady, "Erbium : ytterbium co-doped large-core fiber laser with 297 W continuous-wave output power," IEEE J. Sel. Top. Quantum Electron. **13**(3), 573–579 (2007).
6. M. A. Jebali, J-N. Maran, and S. LaRochelle, "264 W output power at 1585 nm in Er–Yb codoped fiber laser using in-band pumping," Opt. Lett. **39**(13), 3974–3977 (2014).
7. G. Sobon, P. Kaczmarek, A. Antonczak, J. Sotor, and K. M. Abramski, "Controlling the 1 µm spontaneous emission in Er/Yb co-doped fiber amplifiers," Opt. Express **19**(20), 19104–19113 (2011).
8. V. R. Supradeepa, J. W. Nicholson, and K. Feder, "Continuous wave Erbium-doped fiber laser with output power of >100 W at 1550 nm in-band core-pumped by a 1480nm Raman fiber laser," in CLEO: Science and Innovations, OSA Technical Digest (online) (Optical Society of America, 2012), paper CM2N.8.
9. L. V. Kotov, M. E. Likhachev, M. M. Bubnov, O. I. Medvedkov, M. V. Yashkov, A. N. Guryanov, S. Février, J. Lhermite, and E. Cormier, "Yb-free Er-doped all-fiber amplifier cladding-pumped at 976 nm with output power in excess of 100 W," Proc. SPIE **8961**, 89610X (2014).
10. L. V. Kotov, M. Likhachev, M. Bubnov, O. Medvedkov, M. Yashkov, A. Guryanov, S. Fevrier, J. Lhermite, and E. Cormier, "Single-mode Yb-free Er-doped all-fiber laser cladding-pumped at 976 nm with record efficiency of 40 % and output power of 75 W," in 2013 Conference on Lasers and Electro-Optics - International Quantum Electronics Conference, (Optical Society of America, 2013), paper CJ_8_2.
11. E. Wikszak, J. Thomas, J. Burghoff, B. Ortaç, J. Limpert, S. Nolte, U. Fuchs, and A. Tünnermann, "Erbium fiber laser based on intracore femtosecond-written fiber Bragg grating," Opt. Lett. **31**(16), 2390–2392 (2006).

#327030 https://doi.org/10.1364/OE.26.022378
Journal © 2018 Received 28 Mar 2018; revised 10 Jul 2018; accepted 21 Jul 2018; published 15 Aug 2018

Optics EXPRESS

12. R. S. Quimby, W. J. Miniscalco, and B. Thompson, "Clustering in erbium-doped silica glass fibers analyzed using 980 nm excited-state absorption," J. Appl. Phys. **76**(8), 4472–4478 (1994).
13. L. V Kotov, M. E. Likhachev, M. M. Bubnov, O. I. Medvedkov, D. S. Lipatov, N. N. Vechkanov, and A. N. Guryanov, "High-performance cladding-pumped erbium-doped fibre laser and amplifier," Quantum Electron. **42**(5), 432–436 (2012).
14. M. Bernier, F. Trépanier, J. Carrier, and R. Vallée, "High mechanical strength fiber Bragg gratings made with infrared femtosecond pulses and a phase mask," Opt. Lett. **39**(12), 3646–3649 (2014).
15. J. Nilsson, B. Jaskorzynska, and P. Blixt, " Implications of pair-induced quenching for erbium-doped fiber amplifiers," in Optical Amplifiers and Their Applications, 1993 OSA Technical Digest Series (Optical Society of America, 1993), paper MD19.
16. T. Georges, E. Delevaque, M. Monerie, P. Lamouler, and J.-F. Bayon, "Pair induced quenching in erbium doped silicate fibres," in Optical Amplifiers and Their Applications, 1992 OSA Technical Digest Series (Optical Society of America, 1992), paper WE4.
17. T. Erdogan, V. Mizrahi, P. J. Lemaire, and D. Monroe, "Decay of ultraviolet-induced fiber Bragg gratings," J. Appl. Phys. **76**(1), 73–80 (1994).
18. Bernier, M., R. Vallée, B. Morasse, C. Desrosiers, A. Saliminia, and Y. Sheng. "Ytterbium fiber laser based on first-order fiber Bragg gratings written with 400nm femtosecond pulses and a phase-mask," Opt. Express **17**(21), 18887–18893 (2009).
19. W. J. Miniscalco, "Erbium-doped glasses for fiber amplifiers at 1500 nm," J. Lightwave. Technol. **21**(9), 234–250 (1991).

1. Introduction

High power laser sources operating in the 1.5 to 1.7 μm spectral region are of interest for many applications, such as light detection and ranging (LIDAR) [1], spectroscopy and optical wireless communication systems [2], a demand further fostered by the "eye-safe" quality of this spectral band [3]. In turn, single-mode all-fiber laser cavities offer undeniable benefits for out-of-lab deployment, notably robustness, reliability, compact design and excellent beam quality. However, the large-scale implementation of high performance fiber lasers is hampered by the substantial growth of costs and increased fabrication times tied to power-scaling. As such, it is of large commercial appeal to simplify the fabrication process of such lasers while maximizing performance.

The 1.5 to 1.7 μm spectral band has been the subject of extensive work in the past due to its concordance with the high-transmission window of silica-glass fibers. To date, Lin *et al* have demonstrated the highest power emitted by a fiber laser in this wavelength range, reaching 656 W [4] with an erbium-doped ytterbium-free fiber laser. However, their design was not all-fiber and employed a multimode fiber (V=23), resulting in a poor beam quality ($M^2 \approx 10.5$). Jeong *et al*. have also made a high power demonstration from a fiber laser in this wavelength range, with nearly 300 W of emission at 1567 nm from an erbium-ytterbium co-doped fiber laser [5], but the reliance on free-space elements and an ytterbium co-lasing mechanism complexifies their design and reduces its efficiency at high power. Similar results were obtained by Jebali *et al* [6], who reached 264 W of output power at 1585 nm with a 74% efficiency using the in-band pumping at 1535 nm of an Er-Yb codoped fiber, but employed a complex pumping scheme involving 36 combined 14 W lasers to achieve this performance. Given the 1 μm light emitted as a consequence of including ytterbium in the lasing scheme, which can be hazardous to both the human eye and optical devices [7], it is of interest for a number of applications to develop sources without this co-dopant. With the use of an ytterbium-free erbium fiber laser, Supradeepa et al. have reached 100 W of average power at 1554 nm with an efficiency of 71% with respect to the absorbed 1480-nm pump [8]. However, this in-band pumping scheme required a complex and costly Raman fiber laser, resulting in a poor overall electrical-to-optical efficiency. A simple all-fiber amplifier was presented by Kotov *et al*. using multi-mode clad-pumping of a singly Er-doped fiber to amplify a 1585 nm signal to 103 W [9], but its amplifier-based design forced the use of a 4 W seed laser to get the desired output, resulting in a limited pump absorption, thus limited overall efficiency and scalability. Using their optimized fiber design, the same group

Optics EXPRESS

has reported a 75 W all-fiber laser emitting at 1603 nm at a slope efficiency near 40% using a fiber Bragg grating (FBG) [10]. Although such results highlight that singly-doped erbium fiber lasers can operate at both high power and efficiency, the laser design was not splice-less and its assembling process could still be further simplified. A known method of further simplifying fiber lasers is to use FBGs written directly in the gain fiber. Wikszak *et al*. have made one such demonstration, showing a very simple design using a FBG written with 800 nm femtosecond pulses in a nonphotosensitive Er-doped fiber [11]. However, they still used some free-space components and have only demonstrated a low power emission of 38 mW at 1554.5 nm.

In this article, we demonstrate a very simple erbium fiber laser design, monolithically assembled using a commercial multi-mode pump diode emitting at 976 nm and fiber Bragg gratings written directly in the gain fiber through the polymer coating. In sequence, two cladding-pumped laser cavities emitting at 1610 nm were created based on this design: the first with a high erbium concentration, and the second with a doping level reduced to improve laser efficiency.

This paper will first describe the design and characteristics of the erbium-doped fibers, then the assembly and testing of the laser cavities.

2. Fiber fabrication and properties

In order to maximize optical efficiency, a high erbium concentration in the fiber is desired to increase the pump absorption. However, high erbium concentrations lead to the formation of detrimental erbium ion clusters which reduce the lifetime of the upper energy level and hinder laser emission [12]. As such, common practice is to employ aluminum as a co-dopant to improve erbium solubility and limit clustering. For the present experiment, two silica glass preforms were created using the MCVD technique and doped with the solution doping process, each containing a different concentration of Er_2O_3 and Al_2O_3 in the core (see Table 1). The first preform is highly doped to test the effects of a high erbium concentration, while the erbium concentration of the second preform is selected based on previous work by Kotov *et al.* [9] to improve laser efficiency.

To ensure compatibility with commercially available high-power pump diodes, a cladding diameter of 125 to 130 µm was targeted for the fibers. Core/clad aspect ratio in each preform was maximized to improve pump absorption [13], while maintaining a core size small enough to ensure single-mode operation in the 1.5 to 1.7 µm wavelength range (given the resulting NA of each fiber core). Both preforms were polished on two sides into a "double D" shape to favor pump absorption by inhibiting the propagation of poorly interactive circular modes. The preforms were then drawn into fibers and coated with a low-index fluoroacrylate polymer using in-house facilities at COPL.

Table 1 summarizes the fiber parameters, and Fig. 1 shows a picture of the cross-section of each fiber. Cutoff values were measured using the bend reference technique, attenuation (α) measurements were obtained via cutback, and the numerical aperture is calculated from the cutoff and core size values. The proportion of paired erbium ions is obtained from corresponding simulations and explained in section 3. As can be seen in the table, a higher erbium concentration largely increases the pump absorption and raises the core's refractive index, thus forcing a reduction in core size to maintain a cutoff wavelength below 1500 nm.

3. Laser assembly and characterization

A schematic of the monolithic laser cavity design used in this work is presented in Fig. 2. As the system relies on clad-pumping, the junction with the diode pigtail is a standard multi-mode splice that can be easily accomplished with an arc splicer (Fujikura, model FSM-100P). Fiber Bragg gratings (FBG) serve as reflectors at the signal wavelength and are written in the gain fiber directly through the polymer coating using an 800 nm femtosecond laser and the phase-mask technique, as described in [14]. The gain fiber is spooled around a metal cylinder for passive cooling. A 4^o angled cleave at the fiber output reduces undesirable feedback from Fresnel reflections. Overall,

Optics EXPRESS

Table 1. Parameters of the two fibers fabricated for this experiment

Parameter	Fiber 1	Fiber 2
Core diameter [µm]	12	16
Cladding diameter [µm]	125	129
Cutoff wavelength [nm]	1452	1480
Numerical aperture	0.09	0.07
Er_2O_3 concentration [mol.%]	0.36	0.03
Al_2O_3 concentration [mol.%]	0.55	1.2
α_{clad} @976 nm [dB/km]	1100	43.5
α_{core} @1200 nm [dB/km]	23.5	23.1
Estimated % of paired ions ($2k$)	40	9.3

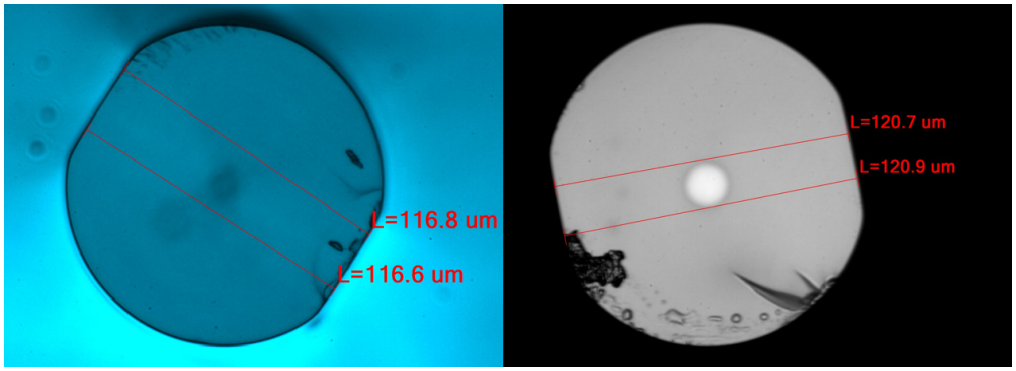

Fig. 1. Optical microscope pictures of the cross-section of fiber 1 (left) and fiber 2 (right).

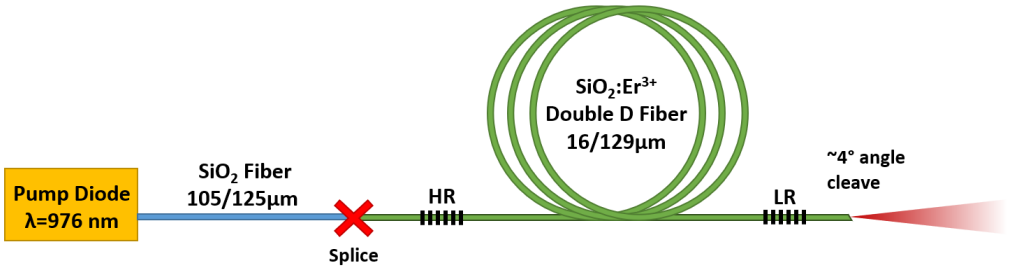

Fig. 2. Laser cavity design used for this work. HR and LR respectively designate a highly-reflective or lowly-reflective fiber Bragg grating. The entrance fiber (blue) is the pigtail of the pump diode.

the simplicity of the design and the absence of free-space components make this laser cavity very quick to assemble and suitable for large volume production. Note that while a high index polymer could be applied to the end section of the fiber (stripped of coating) to remove leftover in-clad pump power from the output, a dichroic filter is used instead for output separation so as to allow individual measurements of both the residual pump and the 1610 nm signal for this study.

Two laser cavities were assembled using this design, one for each of the studied fibers. In both cases, an HR-FBG (highly reflective FBG at the cavity entrance) having a reflectivity above 99% is targeted to maximize laser efficiency. The laser output wavelength of 1610 nm was selected

Optics EXPRESS

to obtain maximum gain after analyzing the amplified spontaneous emission spectra at long cavity lengths, which showed in both fibers a natural tendency to amplify this wavelength range. To direct the choice of the LR-FBG (low reflectivity FBG at the cavity output) reflectivity and cavity length for both fibers, the effect of each of these parameters was tested experimentally by constructing cavities of different lengths, testing their optical efficiency, then using thermal annealing to lower the LR-FBG reflectivity without affecting the pump injection. So as to ensure experimental consistency and safe testing at short cavity lengths, this parametric study was performed at a relatively low pump power (<30 W). As an example of this process, Fig. 3 shows some of the optical efficiencies obtained in this manner using various parameter values and fiber 2. To get a better understanding of the cavity dynamics, a numerical simulation model based on the formalism proposed by Nilsson *et al.* [15] is developed concurrently with the experimental study to estimate the pair-induced quenching (PIQ) in both fibers. An outline of this model is available in Appendix A.

Figure 3 suggests that the highest efficiency is obtained by using minimal LR-FBG reflectivity (~1%) and, in the case of fiber 2, a fiber length near 60 m. Both of these results can be attributed in major part to the formation of erbium ion pairings, which leads to non-saturable absorption and the non-radiative de-excitation of the $^4I_{13/2}$ erbium energy level involved in the laser transition [16]. As such, a longer cavity length re-absorbs the signal being generated and turns part of it into heat, while a short cavity fails to absorb enough pump to maximize the signal output. It should be noted that at low pump power (i.e. low temperature), the wavelength-stabilized diode used to pump fiber 2 is known to emit some power off-peak (around 965 nm), thus reducing overall pump absorption. This causes the parametric study to underestimate the efficiency of the final cavity, and is accounted for in simulations by adjusting the pump absorption cross-section to an effective value that matches the observed data, as shown on Fig.3.

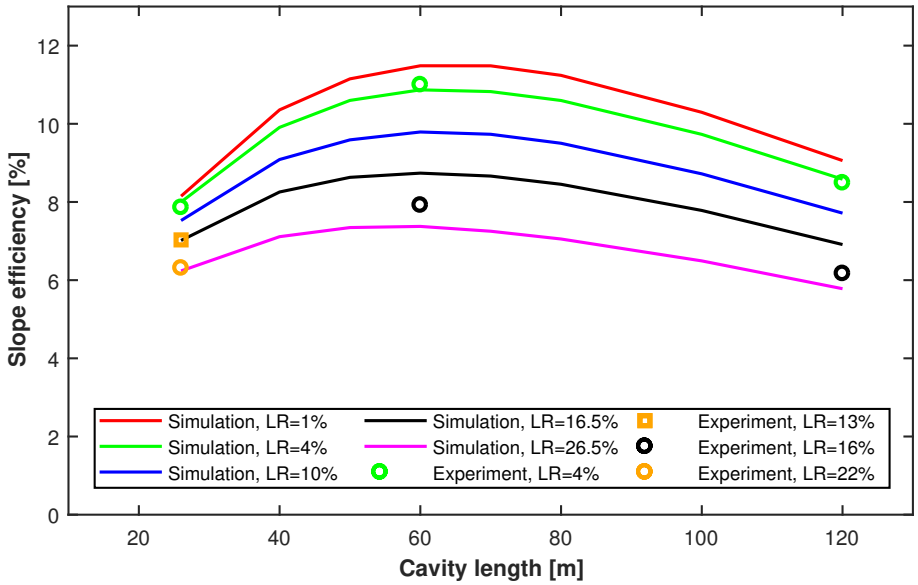

Fig. 3. Slope efficiency with respect to launched pump power obtained with different laser cavity configurations using fiber 2. Both simulated and experimental results (non-exhaustive) are presented, for varying values of cavity length and LR-FBG reflectivity. These tests were carried out at pump powers under 30 W.

The first cavity is built using fiber 1. The cavity length is 3.1 m from the HR-FBG to the LR-FBG, with a few extra centimeters on both ends for splicing and cleaving. HR-FBG and

Optics EXPRESS

LR-FBG reflectivity are 99% and 4%, respectively. The laser was pumped by a BWT K980DA5RN diode emitting at 976 nm. In this first cavity, precise pump wavelength control was not necessary considering the fiber's large pump absorption of 1.1 dB/m and the purpose of this test. Figure 4 shows the signal and residual pump power at the output of this laser as a function of launched pump power. Despite the optimization of the fiber length and LR-FBG reflectivity, the laser efficiency with respect to the absorbed pump power is only about 7% . Moreover, only one third of the launched pump power is absorbed. This is due to the re-absorption phenomenon described above, exacerbated by the high erbium concentration, which makes for a very short optimal cavity length. Using our computational model, the proportion of paired ions in this fiber ($2k$) was estimated to be around 40 %, which is indeed much too large for efficient laser operation.

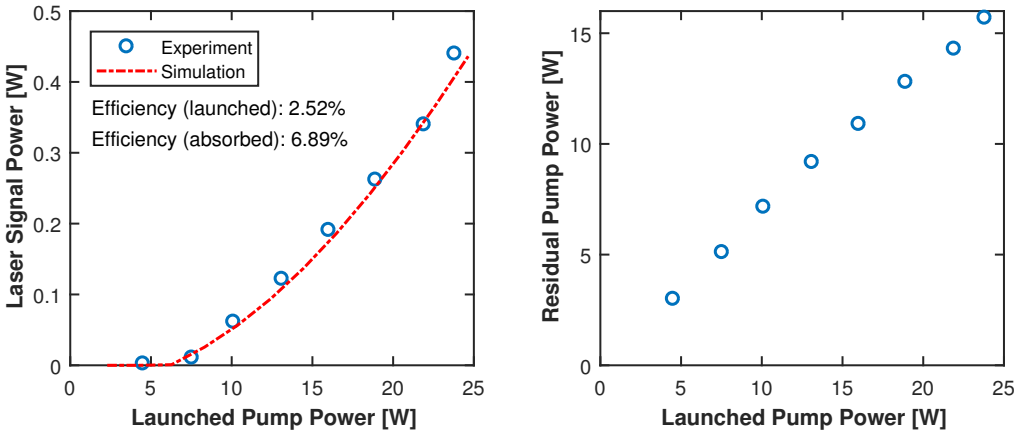

Fig. 4. Output power at the signal (1610 nm, left) and pump (967 nm, right) wavelengths as a function of launched pump power for the laser cavity built with fiber 1. Slope efficiency with respect to both absorbed and launched pump power is identified. The results obtained from simulations (red dotted line) agree well with the experimental results.

The second cavity, made with fiber 2, is pumped with a wavelength-stabilized diode (nLight Element e18) delivering over 120 W of power at 976 nm through a 105/125 µm (core/clad) multimode fiber, allowing consistent targeting of the absorption band at high powers. Based on the experimental study presented in Fig. 3, the cavity has a length of 62 m and the HR-FBG and LR-FBG have a reflectivity of 99.6 % and 1 % respectively at the signal wavelength. Figure 5 (left) displays the full reflection spectrum of each FBG, as measured using a broadband ASE source, an optical circulator and an Optical Spectrum Analyzer (OSA). The laser spectrum at different output powers is also presented in Fig. 5 (right). Next, the output power at the signal and pump wavelengths as a function of launched pump power are measured and displayed on Fig. 6. For this measurement, data points are taken starting from the highest power to ensure even temperature of the system from one point to the next and optimal diode behavior. Lastly, beam quality (M^2) is quantified using an automated optical bench test (Photon Inc. Nanoscan), yielding M^2<1.1 on orthogonal axes as shown on Fig. 7.

The use of fiber 2 results in a longer cavity with significantly improved laser performances. At maximum output, the signal's spectral width is very narrow (FWHM = 0.07 nm), a typical result for FBG-based fiber lasers. A shift of the emission wavelength on the order of ~0.5 nm is noticeable as the power increases to maximum, a consequence of the LR-FBG experiencing thermal expansion. The beam quality is excellent, very close to the diffraction limit, which further confirms the single-mode operation of the laser. At nearly 20 % slope efficiency and 18.3% overall efficiency with respect to launched pump power, and a 21.7 W maximum signal output, this is, to the best of our knowledge, the most powerful splice-less FBG-based all-fiber laser demonstrated

Optics EXPRESS

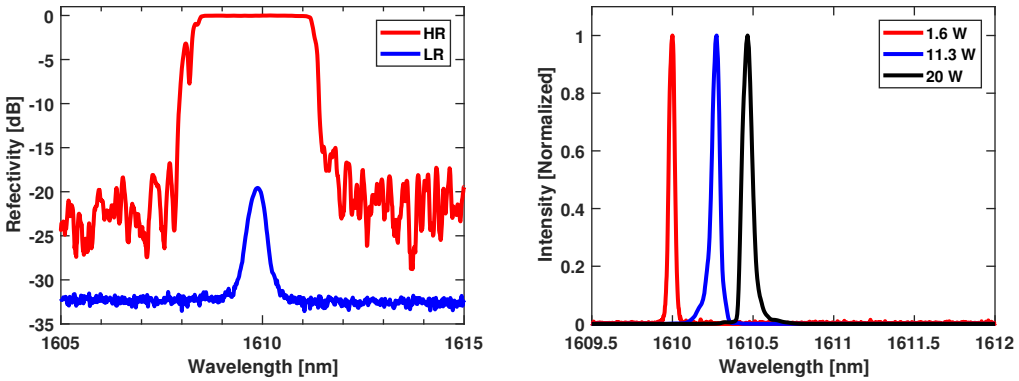

Fig. 5. **Left:** Spectral reflectivity of the FBGs written in the optimized cavity (fiber 2). **Right:** Spectrum of the laser signal emitted by this cavity for different output powers.

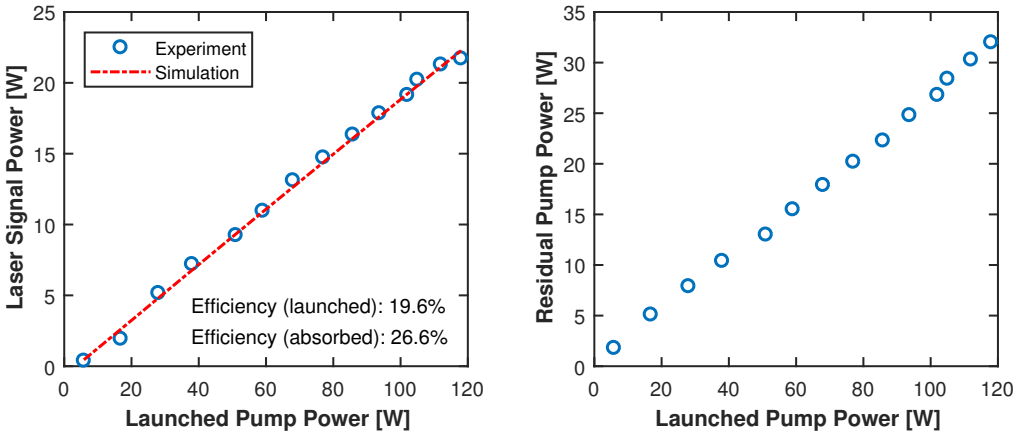

Fig. 6. Power characterization and simulation for the cavity built with fiber 2. Points at low power were taken after heating the diode at high powers beforehand.

at this wavelength. Moreover, the measurements show no sign of gain saturation, implying that combining additional diodes would increase the signal output, though it would also add steps and pieces to the assembling process and likely require improved heat management. Nevertheless, the residual pump measurement shows that nearly a third of the launched pump power is present at the output: efficiency could be significantly increased by improving pump absorption. However, as previously discussed, a longer cavity length actually decreases overall efficiency because of signal re-absorption. This is emphasized on Fig. 8, which shows that the numerical simulation estimates a slightly negative gain near the end of the 62 m cavity. Thus, a more promising way to improve pump absorption would be to enlarge the fiber core size, as proposed and experimentally demonstrated by Kotov *et al.* [9,10,13]. However, such a modification would also require lowering the core NA (e.g. with fluorine doping) in order to maintain single-mode operation. By using such an optimized fiber design, a two-fold increase of the laser efficiency compared with current results is expected. On the other hand, computations suggest that still about 9.3 % of erbium ions are paired in this fiber, indicating that a reduction of the erbium concentration or an increase in the concentration of other dopants (Al or added F) could still have a positive impact on efficiency. Once again, this would come with an adjustment of the core refractive index. Finally, considering the amount of leftover pump, amplifying the current laser using another segment of doped fiber

Optics EXPRESS

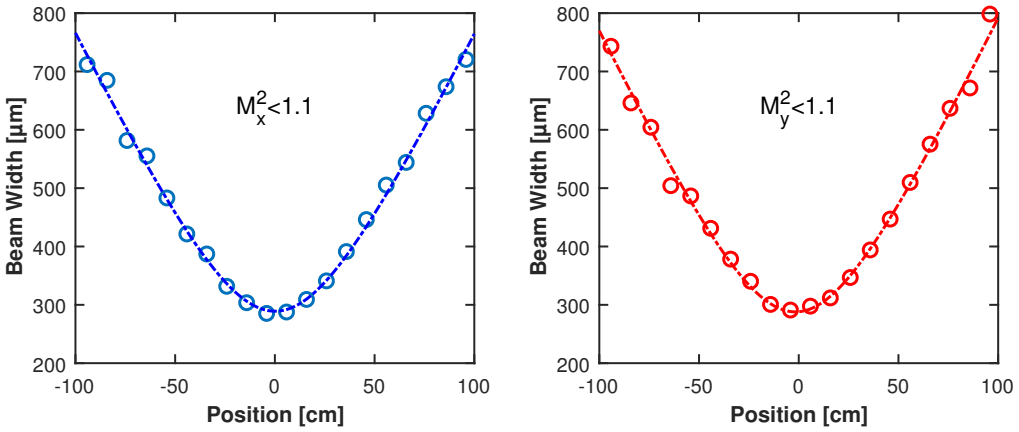

Fig. 7. Beam quality measurement on orthogonal axes. The figure shows beam width at different positions along the optical axis of the measurement bench. The function $w = \sqrt{a + bz + cz^2}$, where w is width and z is position, is fitted to determine the M^2.

could be investigated in the future, though such an addition would complexify the design.

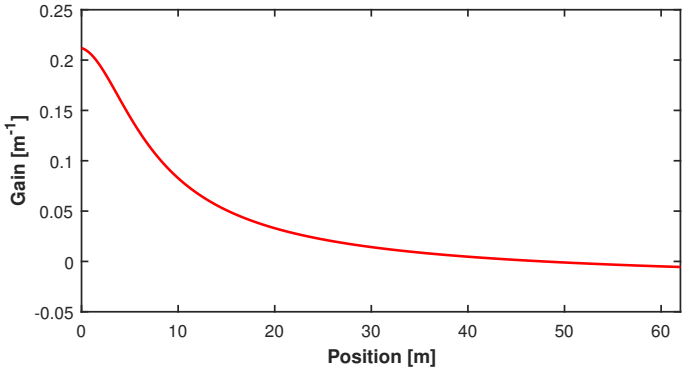

Fig. 8. Simulated distribution of laser gain in the final cavity made with fiber 2. The fiber is pumped from the left side.

As closing remarks, it is worth discussing some of the technicalities surrounding the use of FBGs. Firstly, as previously observed, the peak wavelength of reflection (and, as such, the wavelength of the laser signal) changes with respect to output power through temperature increase. As, in this case, the LR-FBG was simply taped to an aluminum plate for heat dissipation, the wavelength shift could be further mitigated by better managing the heat generated by the laser operation, either by fixing the LR-FBG with a thermal conductor or by reducing its losses. Secondly, FBGs are known to deteriorate with respect to time, slowly reducing in reflectivity [17] and leading to a small variation in laser efficiency. This process can be mitigated by thermally annealing the FBG, heating it up to wipe out the less stable part of its index change. In this case, the FBGs were annealed at a low temperature of 150°C for 10 minutes after writing. This deliberately low temperature was maintained in order to avoid damaging the polymer coating of the fiber. Previous work has shown that annealing FBGs written with femtosecond pulses at high temperatures (up to 500 °C) could nearly nullify their losses [18]. Unfortunately, this level of annealing is not attainable without degrading the polymer coating properties and comes as a trade-off for the simplicity of writing FBGs without removing the polymer coating of the fiber. It

Optics EXPRESS

is worth noting, finally, that despite all the observations raised above, the laser shows very good stability during use once thermal equilibrium has been reached. This is shown on Fig. 9, which displays the signal power registered from the laser near 20 W during a continuous period of 24 hours.

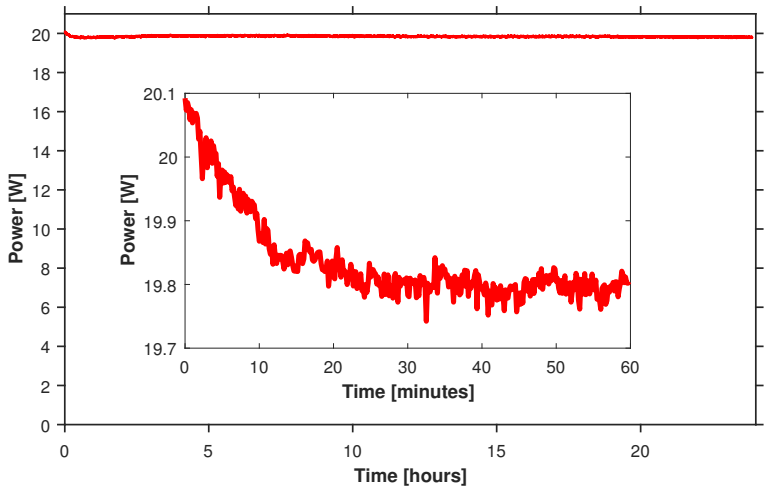

Fig. 9. Stability of the laser signal during 24 hours around 20 W. The inset zooms in on the laser during warm-up.

4. Conclusion

In conclusion, we have designed an effective erbium-doped monolithic fiber laser with a simple assembling process that takes advantage of FBGs written directly in the gain fiber through the polymer coating and clad-pumping from a single commercial pump diode, making steps towards high-volume commercial deployment. The resulting cavity emits a stable, high-quality beam (M^2<1.1) with over 20 W of power in a narrow spectrum centered at a wavelength of 1610 nm, with a slope efficiency of 19.6% with respect to launched pump power. Furthermore, the detrimental effects of pair-induced quenching were demonstrated using a fiber doped with a significantly higher (12x) amount of erbium ions. A numerical model estimated a proportion of paired ions over four times greater in the highly concentrated fiber as opposed to the less doped fiber. Further work will improve the laser efficiency by increasing the pump absorption through an increase of the core size or a modification of dopant concentrations, and focus on developing automation procedures for the large-scale production of similar laser cavities.

Optics EXPRESS

Appendix A: numerical modeling

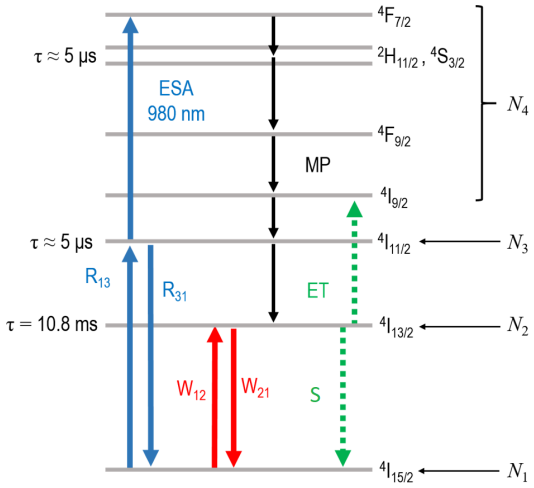

Fig. 10. Energy diagram of the Er^{3+}:SiO_2 system, with transitions. Left are the lifetimes in Al/P silica glass [19] while right are the energy level labels. GSA and ESA are related to the 976 nm pump, S is the laser signal at 1.55 µm, MP is rapid multi-phonon decay and ET is energy transfer. N_i are the energy levels used in the theoretical modeling.

With the intent of improving our understanding of the laser cavity, a computational model was elaborated to simulate an erbium-doped fiber laser. For this purpose, the energy diagram shown in Fig. 10 represents the energy level dynamics. As the upper levels of this diagram relax very quickly compared to the N_2 level (used for lasing), the diagram can be simplified to a system of four levels dynamically described by the following system of equations:

$$\frac{dN_4}{dt} = -\frac{N_4}{\tau_4} + R_{\mathrm{ESA}} \tag{1}$$

$$\frac{dN_3}{dt} = -\frac{N_3}{\tau_3} + \frac{N_4}{\tau_4} + R_{\mathrm{P}} - R_{\mathrm{ESA}} + W_{22}N_2^2 \tag{2}$$

$$\frac{dN_2}{dt} = -\frac{N_2}{\tau_2} + \frac{N_3}{\tau_3} - W_{21} - 2W_{22}N_2^2 \tag{3}$$

$$N_{\mathrm{tot}} = N_1 + N_2 + N_3 + N_4 \tag{4}$$

where N_i and τ_i represent the population and lifetime of a given energy level i, W_{22} is the coefficient of the two-photon energy transfer (ET), and the remaining variables are given by

$$R_{\mathrm{P}} = \frac{\sigma_P \Gamma_P \lambda_P}{hcA_c}\left(N_1 - N_3\right)P_P \tag{5}$$

$$R_{\mathrm{ESA}} = \frac{\sigma_{\mathrm{ESA,abs}} \Gamma_P \lambda_P}{hcA_c} N_3 P_P \tag{6}$$

$$W_{21} = \frac{\Gamma_S \lambda_S}{hcA_c}\left(\sigma_{\mathrm{s,em}} N_2 - \sigma_{\mathrm{s,abs}} N_1\right)P_S \tag{7}$$

where A_c is the effective core area, h is Planck's constants, and σ denotes the absorption (*abs*) or emission (*em*) cross-section of the signal (S), pump (P) or ESA transition. With the same

Optics EXPRESS

subscripts, Γ is the confinement factor, P is laser power and λ is the wavelength.

Next, the model is modified to account for pair-induced quenching of the erbium ions, which is detrimental to the laser efficiency. This is implemented using the method developed by Nilsson *et al.* [15], such that in steady-state the total number of ions N_{tot} is divided in singular and paired populations (N_{tot}^S and N_{tot}^P) according to a proportion k.

$$2k = \frac{N_{\text{tot}}^P}{N_{\text{tot}}} \tag{8}$$

$$N_{\text{tot}}^S = N_{\text{tot}} - N_{\text{tot}}^P \tag{9}$$

Moreover, the paired population of the second erbium energy level (N_2^P) can be related to other quantities via the following equations [15], where the superscripts S and P denote quantities related to singular and paired ions.

$$\frac{dN_2^P}{dt} = -\frac{N_2^P}{\tau_2} + \frac{R_{\text{P}}}{N_1^S - N_3^S} N_1^P - \left[\frac{R_{\text{S}}}{N_2^S} + \frac{R_{\text{P}}}{N_1^S - N_3^S}\right] N_2^P \tag{10}$$

$$N_{\text{tot}}^P = N_1^P + N_2^P \tag{11}$$

Lastly, the simulation is carried out by calculating the propagation of signal and pump power along the fiber:

$$\pm \frac{dP_P^{\pm}}{dz} = -\left[\Gamma_P \left(\sigma_P (N_1^S + N_1^P) + \sigma_{\text{ESA}} N_3^S\right) + \alpha_P\right] P_P^{\pm} \tag{12}$$

$$\pm \frac{dP_S^{\pm}}{dz} = \left[\Gamma_S \left(\sigma_{\text{s,ems}} (N_2^S + N_2^P) - \sigma_{\text{s,abs}} (N_1^S + N_1^P)\right) - \alpha\right] P_S^{\pm} \tag{13}$$

where superscripts + and - denote forward and backward propagation. The whole system of equations is numerically solved by dividing the fiber length and the passage of time in finite elements, and imposing boundary conditions on each end of the cavity that are defined by the input pump and the reflectivity of the FBGs.

Funding

Fonds Québécois de Recherche sur la Nature et les Technologies (FQRNT); Natural Sciences and Engineering Research Council of Canada (NSERC); Canadian Foundation for Innovation (CFI).

Acknowledgments

This research was performed at Université Laval as part of a graduate course (PHY-7052, laboratoire de photonique avancée) taking place in two seperate semesters at the department of Physics, Engineering Physics and Optics. The group would like to thank Pr. Younès Messaddeq for support to the MCVD and fiber drawing processes used for fiber fabrication, as well as Yannick Ledemi, Stéphane Gagnon and Patrick Larochelle for technical assistance.